Physica D 284 (2014) 16–26

Contents lists available at ScienceDirect

Physica D

journal homepage: www.elsevier.com/locate/physd

Large fluctuations of the nonlinearities in isotropic turbulence. Anisotropic filtering analysis

D. Tordella [a,*], S. Di Savino [a], L. Sitzia [b,1]

[a] Dipartimento di Ingegneria Meccanica e Aerospaziale, Politecnico di Torino, Corso Duca degli Abruzzi 24, 10129 Torino, Italy

[b] Dottorato in Statistica e Matematica Applicata, Scuola di Dottorato "V.Pareto" - Universita' di Torino, via Real Collegio 30, 10024 Moncalieri (To), Italy

HIGHLIGHTS

- The article highlights the difference between Navier–Stokes and Kolmogorov turbulence in terms of stretching–tilting statistics.
- Vortex stretching magnitude normalized over the local enstrophy $= f$.
- Near zero probability for stretching of intensity larger than twice the enstrophy.
- Anisotropic filtering proposed for targeting different structure kinds.
- Inertial range blobs filtered out: f increases; larger ones filtered out: f falls.

ARTICLE INFO

Article history:
Received 2 May 2013
Received in revised form
17 April 2014
Accepted 1 May 2014
Available online 11 June 2014
Communicated by M. Vergassola

Keywords:
Stretching–tilting
Navier–Stokes turbulence
K41
Anisotropic filtering
Phase randomization
Blob

ABSTRACT

Using a Navier–Stokes isotropic turbulent field numerically simulated in a box with a discretization of 1024^3 (Biferale et al., 2005), we show that the probability of having a stretching–tilting larger than a few times the local enstrophy is low. By using an anisotropic kind of filter in the Fourier space, where wavenumbers that have at least one component below a threshold or inside a range are removed, we analyze these survival statistics when the large, the small inertial or the small inertial and dissipation scales are filtered out. By considering a flow obtained by randomizing the phases of the Fourier modes, and applying our filtering techniques, we identified clearly the properties attributable to turbulence.

It can be observed that, in the unfiltered isotropic Navier–Stokes field, the probability of the ratio $(|\boldsymbol{\omega}\cdot\nabla\mathbf{U}|/|\boldsymbol{\omega}|^2)$ being higher than a given threshold is higher than in the fields where the large scales were filtered out. At the same time, it is lower than in the fields where the small inertial and dissipation range of scales is filtered out. This is basically due to the suppression of compact structures in the ranges that have been filtered in different ways. The partial removal of the background of filaments and sheets does not have a first order effect on these statistics. These results are discussed in the light of a hypothesized relation between vortical filaments, sheets and blobs in physical space and in Fourier space. The study in fact can be viewed as a kind of test for this idea and tries to highlight its limits. We conclude that a qualitative relation in physical space and in Fourier space can be supposed to exist for blobs only. That is for the near isotropic structures which are sufficiently described by a single spatial scale and do not suffer from the disambiguation problem as filaments and sheets do.

Information is also given on the filtering effect on statistics concerning the inclination of the strain rate tensor eigenvectors with respect to vorticity. In all filtered ranges, eigenvector 2 reduces its alignment, while eigenvector 3 reduces its misalignment. All filters increase the gap between the most extensional eigenvalue $\langle\lambda_1\rangle$ and the intermediate one $\langle\lambda_2\rangle$ and the gap between this last $\langle\lambda_2\rangle$ and the contractile eigenvalue $\langle\lambda_3\rangle$. When the large scales are missing, the modulus of the eigenvalue 1 becomes nearly equal to that of the eigenvalue 3, similarly to the modulus of the associated components of the enstrophy production.

1. Introduction

The formation of spatial and temporal internal scales can in part be associated to the stretching and tilting of vortical structures. Many aspects of the behavior of turbulent fields have been

* Corresponding author.
E-mail address: daniela.tordella@polito.it (D. Tordella).
URL: http://www.polito.it/philofluid (D. Tordella).

[1] Present address: Risk Methodologies, Group Financial Risk, UniCredit S.p.A., Piazza Gae Aulenti, 20154 Milano, Italy.

http://dx.doi.org/10.1016/j.physd.2014.05.001
0167-2789/

associated to this phenomenon: the onset of instability, vorticity intensification or damping, production and dissipation or the three-dimensionalization of the flow field [1–5]. In the standard picture of turbulence, the energy cascade to smaller scales is interpreted in terms of the stretching of vortices due to the interaction with similar eddy size (see for example [6]). A number of statistical details on the stretching phenomenon and the closely related enstrophy production can be found in the monography by Tsinober (2001, see in particular Chapter 6, [7]).

Although the important physical role of these inertial phenomena is recognized, the literature does not often include statistical information on quantities such as the magnitude or the components of $\boldsymbol{\omega} \cdot \nabla \mathbf{U}$. For instance, in a letter to Nature (2003) dedicated to the measurements of intense rotation and dissipation in turbulent flows, Zeff et al. [8] observe that the understanding of the temporal interactions between stretching and vorticity is crucial to the science of extreme events in turbulence. However, the statistics presented there concern dissipation and enstrophy and not directly stretching. The literature more often includes statistical information concerning other gradient quantities such as the strain rate or the rate-of-rotation tensors, and, in particular, their fundamental constituents: the longitudinal or transverse velocity derivatives. The skewness and flatness factors of the velocity derivative have been considered in a number of laboratory and numerical studies. For instance, Batchelor and Townsend in 1949 [9], through the study of the oscillograms of the velocity derivatives, showed that the energy associated with large wave numbers is very unevenly distributed in space. More recently it has been shown how velocity derivatives increase monotonically with the Reynolds number, see e.g. [10,11], and the reviews by Sreenivasan and Antonia (1997) [12] and Ishihara, Gotoh and Kaneda (2009) [13]. In particular, Ishihara et al. [14], considering one-point statistics of velocity gradients and Eulerian and Lagrangian accelerations analyzed the data from high-resolution direct numerical simulations (DNS) of turbulence in a periodic box, with up to 4096^3 grid points, and found for these gradients an algebraic dependence on Re_λ.

One-point statistics of velocity gradients and Eulerian and Lagrangian accelerations are studied by analyzing the data from high-resolution direct numerical simulations (DNS) of turbulence in a periodic box, with up to 4096^3 grid points.

In the case of turbulent wall flows, laboratory measurements of both the mean and the r.m.s. of fluctuations of the stretching components across the two-dimensional boundary layer have been reported by Andreapoulos and Honkan (2001) [15]. In this study, the normalized r.m.s values of the stretching components are very significant throughout the boundary layer and reach values that are one order of magnitude larger than the mean span-wise component (the only significant mean component, however and only in the near wall region). The values observed for the r.m.s. of the stretching range from 0.04, close to the wall, to about 0.004 in the outer part.

In a study concerning the structure and dynamics of vorticity and rate of strain in incompressible homogeneous turbulence, Nomura and Post (1998) [16] demonstrate the significance of both local dynamics (influence of local vorticity) and spatial structure (influence through non-local pressure Hessian) in the interaction of the vorticity and strain rate tensor. The behavior of high-amplitude rotation-dominated events cannot be solely represented by local dynamics due to the formation of distinct spatial structure. Instead, high-amplitude strain dominated regions are generated predominantly by local dynamics. The associated structure is less organized and more discontinuous than the one associated with rotation dominated events. They conclude that non-local effects are significant in the dynamics of small scale motion. This should be considered in the interpretation of single-point statistics. Characterizations of small-scale turbulence should consider not only the typical structures there present but also typical structure interactions. In this context these authors offer the radial distribution of the magnitude of the strain rate tensor normalized on the enstrophy. In this paper the maximum value of this magnitude is found close to 0.2.

Laboratory statistical information on the stretching of field lines can be found in [17]. Here, probability density functions of the logarithm of the local stretching in N cycles were obtained for several two-dimensional time-periodic confined flows exhibiting chaotic advection. The stretching fields were observed to be highly correlated in space when N is large, and the probability distributions were observed to be similar for different flows.

However, a few examples in literature can also be cited regarding direct results for stretching–tilting statistics. For instance, recently experimental and numerical confirmation has been found of the predominance of three dimensional turbulent vortex stretching in the positive net enstrophy production. These aspects have been extensively considered in Tsinober (2000) [18] and in the 2001 monography [7], where a number of statistical geometrical details concerning the vortex alignment, compression, tilting, and folding are outlined. Through two papers, Constantin, Procaccia and Segel (1995) [19], Galanti, Procaccia and Segel (1996) [20] consider the stretching and its relationships with the amplification of vorticity and the straightening of the vortex lines. They show that the same stretching that amplifies the vorticity also tends to straighten out the vortex lines. They also show that in well-aligned vortex tubes, the self-stretching rate of the vorticity is proportional to the ratio of the vorticity and the radius of curvature. In this context [20] gives statistics on the stretching and vortex line curvature. Numerically this is seen as the appearance of high correlations between the stretching and the straightness of the vortex lines. Regarding to this issue, an important universal feature of fully developed turbulent flows is the preferential alignment of vorticity along the eigendirection of the intermediate eigenvalue of the strain-rate tensor. A number of works both experimental and numerical studies on this result are available (Tsinober, Kit and Dracos (1992) [10], Kholmyansky, Tsinober and S. Yorish (2001) [21], Gulitski et al. (2007) [22–24] and Chevillard et al. (2008) [25]). It should be noticed, however, that in the case of *nonlocal* strain rate, Hamlington, Schumacher and Dahm [26], have observed a direct assessment of vorticity alignment with the most extensional eigenvector by using data from highly resolved direct numerical simulations.

In the present study, for the case of isotropic turbulence ($Re_\lambda = 280$ [27]), we consider statistics related to the intensity of the stretching term in the equation for vorticity. If we consider the general instantaneous local intrinsic anisotropy of turbulent fields, looking at stretched structures as filaments and sheets, we would like to be able to disentangle them to follow and understand better their evolution and detailed dynamics. Isotropic filtering is unable to carry out this job.

We have conceived a probe function, the ratio between the magnitude of the vortex stretching and the enstrophy, to empirically and statistically measure the local activity of the stretching phenomenon (see Section 2). In addition, we propose an alternative to the commonly used isotropic filter: the cross filter. This is a new empirical, and at the moment limited, attempt to introduce an anisotropic filtering. In Section 3, we analyze the survival function of the normalized stretching by using the cross filter acting directly on the velocity Fourier space. We do this in the hope of qualitatively highlighting aspects related to the role of the three-dimensional structures known as blobs, sheets and filaments and their hypothetical Fourier counterparts. This study can be viewed as a kind of test for this idea and tries to highlight its limits. To check the implication of the filtering analysis, we quantified for each estimator considered an approximately Gaussian reference velocity field

which has a near K41 structure [28,29]. The phase randomization procedure, which consists in replacing the phase of each individual Fourier mode by a number uniformly distributed in the [0, 2pi] interval, eliminates the asymmetry of the distributions, and significantly reduces the intermittency of the original velocity field obtained by solving the NS equations. Concluding remarks are made in Section 4.

2. The normalized vortex stretching–tilting function

With reference to the phenomena described by the inertial nonlinear nonconvective part of the vorticity transport equation, let us introduce a local measure of the process of three-dimensional inner scales formation

$$f(\mathbf{x}, t) = \frac{|\boldsymbol{\omega} \cdot \nabla \mathbf{U}|}{|\boldsymbol{\omega}|^2}(\mathbf{x}, t) = \frac{|\omega_j S_{ij}|}{|\boldsymbol{\omega}|^2}(\mathbf{x}, t) \tag{1}$$

where $\mathbf{U}$ is the velocity field, S_{ij} is the strain rate tensor, and $\boldsymbol{\omega}$ is the vorticity vector. The numerator, the so called stretching–tilting term of the vorticity equation, is zero in two-dimensional flows. In 3 D fields, it is commonly believed to be responsible for the transfer of the kinetic energy from larger to smaller scales (positive or extensional stretching) and vice versa (negative or compressional stretching). According to definition (1), f depends on the local instantaneous velocity and vorticity fields. In this study, we leave aside the peculiarity associated to the convective forcing and focus on the action of the fluctuation field only. For simplicity, we consider here the fluctuation of a homogeneous isotropic turbulent field [27]. Since the stretching term plays an important role in the enstrophy production, in the previous definition the normalization by $|\boldsymbol{\omega}|^2$ was adopted.

In order to look for the typical range of values of $f(\mathbf{x})$ and in order to relate these last to the behavior of the various structures present in a turbulent field, the function f was evaluated in an incompressible isotropic field which is maintained stationary on average. Moreover, to check the implication of the filtering analysis, we quantified for each estimator considered in the following an approximately Gaussian reference velocity field which has a near K41 structure [28,29]. This is obtained by randomizing the phase of the Fourier transform using a uniform distribution, see for instance [30,31].

The dataset consists of 1024^3 resolution grid point Direct Numerical Simulation (DNS) of an isotropic Navier–Stokes forced field at Reynolds $Re_\lambda = 280$ [27]. Each instant in the simulation is statistically equivalent, and provides a statistical set of a little more than 10^9 elements. We considered the statistics that were obtained averaging over the full domain in one instant. The field has been slightly modified in order to filter out instantaneous effects of the forcing, in other words, a turbulent kinetic energy inhomogeneity of about 20% (in the spatial coordinate system). As this bias was generated by the energy supply at the large scale range, the two largest scales have been filtered out. The resolved part of the energy spectrum extends up to $k \sim 330$. The inertial range extends from $k \sim 10$ to $k \sim 70$, see the compensated version of the 3D spectrum in Fig. 1. The higher wave-numbers, which are affected by the aliasing error, are not shown.

We focus now on a few statistical properties of $\frac{\boldsymbol{\omega}\cdot\nabla\mathbf{U}}{|\boldsymbol{\omega}|^2}$. The pdf of the components of this vector (which are statistically equivalent, since the field is isotropic) is shown in Fig. 4. Symmetry with the vertical axis is expected because of isotropy; the skewness is in fact approximately 10^{-2}, which is not meaningfully far from zero. However, the distribution cannot be approximated with a *Gaussian* function. In fact, the actual kurtosis is approximately 55, which is very far from the Gaussian value of 3.

The range of values attained by $f(\mathbf{x})$ is wide. Values as high as a few hundreds were observed at a sparse spatial points. In order

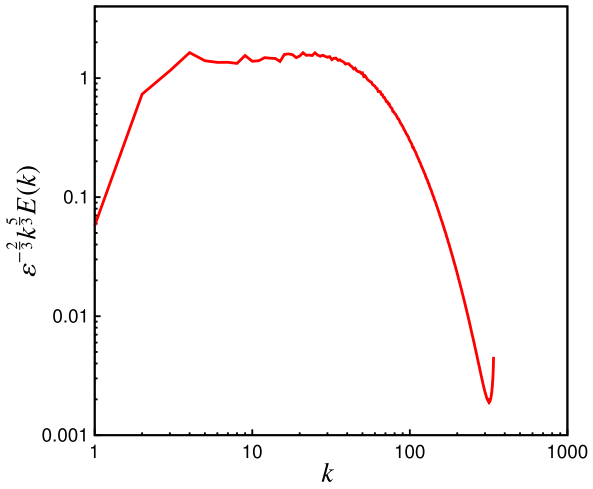

Fig. 1. Compensated 3D energy spectrum of one time instant of the turbulent isotropic field here considered. Open access database http://mp0806.cineca.it/icfd.php. Navier–Stokes direct numerical simulation in a box with a discretization of 1024^3, $Re_\lambda = 280$, see [27].

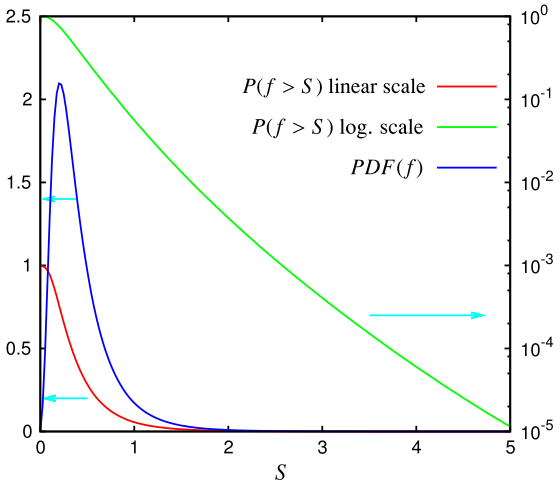

Fig. 2. Survival probability of the normalized stretching–tilting function in a fully resolved isotropic 3D turbulent field $P(f(\mathbf{x}) \geq s)$, $Re_\lambda = 280$. Unfiltered velocity field. The dashed vertical line indicates the value of f where the probability density function is maximum.

to read the typical values of $f(\mathbf{x})$, we study its *survival function*. By denoting $F(s) = P(f(\mathbf{x}) \leq s)$ the cumulative distribution function (cdf) of $f(\mathbf{x})$, the survival function is defined as the complement to 1 of the cdf,

$$S(s) = P(f(x) > s) = 1 - F(s). \tag{2}$$

For each threshold s, $S(s)$ describes the *probability that* $f(\mathbf{x})$ *takes greater values than* s.

It has been found that, when $f(\mathbf{x})$ is evaluated on a well resolved isotropic turbulent field, the probability that $f(\mathbf{x}) > 2$ is low, that is of the order of 10^{-3}, see Fig. 2. Thus, statistically, for $f(\mathbf{x})$, the probability to take small values and values of order 1 is high and moderately high, respectively.

3. Statistics of the normalized vortex stretching–tilting term: analysis on the anisotropically filtered field

By means of suitable convolutions, the application of filters to the velocity field allows the behavior of the function $f(x)$ to be studied in relation to the different turbulence scale ranges. This analysis is carried out using two spectral filters, a high pass and

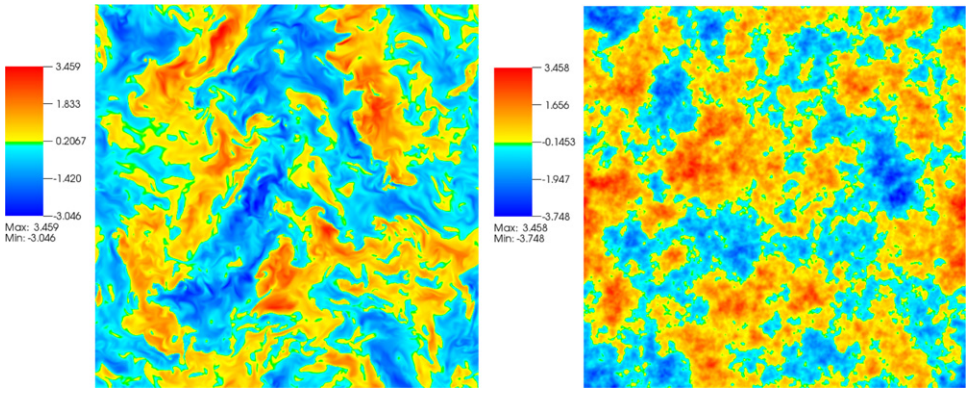

Fig. 3. (Left panel) Visualization of one component of the velocity field in a section parallel to a face of the cube (Navier–Stokes direct numerical simulation in a box with a discretization of 1024^3, $Re_\lambda = 280$. (Right panel) Visualization of the same component of the randomized velocity field in the same section of the computational domain.

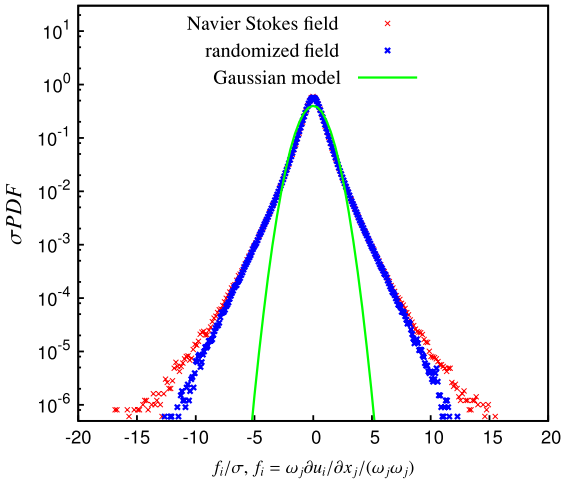

Fig. 4. PDF of the components of the vector $\boldsymbol{\omega} \cdot \nabla \mathbf{u}/|\omega|^2$. Comparison of the unfiltered physical field (red crosses, $S = -4.81 \times 10^{-2}$, $K = 8.76$, variance $= 8.96 \times 10^{-2}$) with the Gaussian model (green line, $S = 0$, $K = 3$, variance $= 8.96 \times 10^{-2}$), and with the randomized field (blue crosses, $S = -1.60 \times 10^{-2}$, $K = 7.46$, variance $= 0.193$). The pdf's are normalized on the standard deviation.

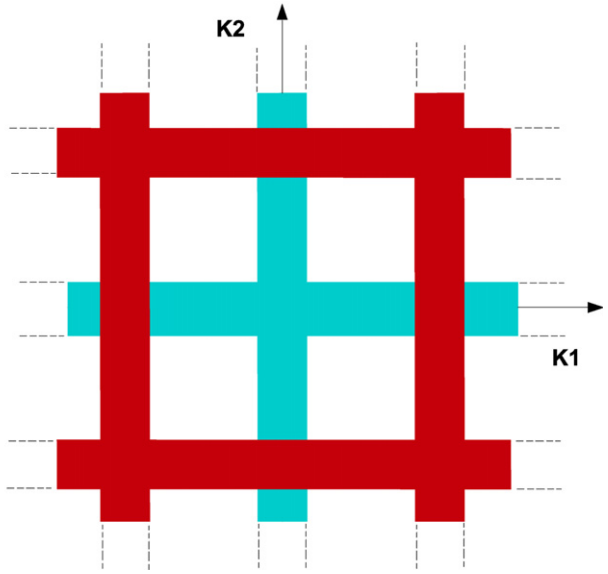

Fig. 5. Scheme of the anisotropic filter here named as CROSS filter. Blue region: high-pass filter, the wave-numbers under a certain threshold are partially removed, see Eq. (4), Red region: band-stop filter, the wave-numbers inside a range are cut, see Eq. (5).

a band-stop filter. To focus in an empirical way on the three principal kind of geometrical structures observed in turbulence, filaments, sheets and blobs, we use here a highly anisotropic kind of filter, which is less traditional than the axisymmetric-type filter. Of course, given the inadequacy of the spectral representation to account for the complex three-dimensional geometry of the turbulent structures commonly seen through visualization tools, the approach we use here is not rigorous and should be considered no more than propaedeutical.

To reason on the implication of the filtering on the flow. In particular, the implication of the filtering on the survival probability. The best way to check the true implication of the filtering is to study, as a reference, a near Gaussian velocity, that has K41 structure, with no structures, no energy transfer, no intermittency, no preferential vorticity alignment. To do so, we have taken the present velocity field and randomized the phase of the Fourier transform using a uniform distribution while respecting the periodicity, see the visualization in Fig. 3. The resulting field is not perfectly Gaussian, but it has a lower skewness and kurtosis, thus it is less intermittent and has a less intense energy transfer of the Navier–Stokes field, see Table 1. It has no preferential vorticity alignment, see Fig. 12. In fact, the pdf of the alignment of the vorticity components with the eigenvectors of the strain rate tensor is perfectly flat and feels only a little the filtering effects, see Fig. 12.

The first kind of filter here used is a sort of high-pass filter, which we refer to as cross filter and which allows to remove the contribution of the structures that are characterized by at least one large dimension. From the Fourier point of view, this means that the structures whose wave-vector has at least one small component are filtered out. One can here think about elongated structures as filaments and sheets or very large globular structures. In Fig. 5, a graphical scheme of the filtering in the wave number plane k_1, k_2 can be seen. The cross filter is here represented in blue. One can see that is a high-pass filter which affects all wave-numbers that, along any possible direction, have at least one component under a certain threshold. Given the threshold k_{MIN}, the filter reduces the contribution of the modes with wave number components

$$k_1 < k_{MIN} \quad \text{or} \quad k_2 < k_{MIN} \quad \text{or} \quad k_3 < k_{MIN}. \tag{3}$$

The representation of this high-pass filter, g_{hp}, can be given by a function of the kind [32]

$$g_{hp}(\underline{k}) = \prod_i \phi(k_i; k_{MIN}), \qquad \phi(k_i, k_{MIN}) = \frac{1}{1 + e^{-(k_i - k_{MIN})}}. \tag{4}$$

Since function g_{hp} filters any wavenumber that has at least one component lower than the threshold k_{MIN}, it reduces the kinetic energy of the filamentous (one component lower than k_{MIN}), layered (two components lower than k_{MIN}) and blobby (three components lower than k_{MIN}) structures. This filter is efficient in reducing the integral scale of the turbulence [32].

Table 1
Field statistics on a single time instant of the components of the velocity, vorticity and normalized vortex stretching vectors. $Re_\lambda = 280$, number of grid points 1024^3. The computational box is 2π wide and the longitudinal correlation length is 1.4. The velocity is normalized on its standard deviation. The randomization is carried out on the velocity field. The small decrease from 1 to 0.989 of the standard deviation for the randomized velocity field measures the numerical accuracy of the phase-randomization procedure. The slight departure from zero for the mean and skewness values (from 3 for kurtosis values) are due to effects associated to the low wave number forcing used to maintain steady the isotropic turbulence and to the numerical error associated to the computation of the vorticity and normalized stretching from the velocity field. The effect of the forcing is mainly felt in the velocity skewness and less in the spatially differentiated quantities where the statistical weight of high wave numbers is higher. The numerical error related to exponentiation, spatial differentiation, etc. instead it is more important for the statistics on the vorticity and the vortex stretching.

		Mean	Variance	Stand.Dev.	Skewness	Kurtosis
U_i	Physical field	-1.40×10^{-6}	1	1	5.25×10^{-2}	3.08
	Random field	-3.37×10^{-6}	0.978	0.989	2.21×10^{-2}	3.03
$f_i = (\omega_j \partial_j U_i)/\lvert\boldsymbol{\omega}\rvert^2$	Physical field	-1.88×10^{-4}	8.96×10^{-2}	0.299	-4.81×10^{-2}	8.76
	Random field	-2.23×10^{-4}	0.193	0.439	6.59×10^{-3}	7.14
ω_i	Physical field	-1.57×10^{-3}	3.42×10^{2}	18.49	-7.02×10^{-2}	9.67
	Random field	3.82×10^{-4}	2.63×10^{2}	15.4	3.55×10^{-4}	3.06

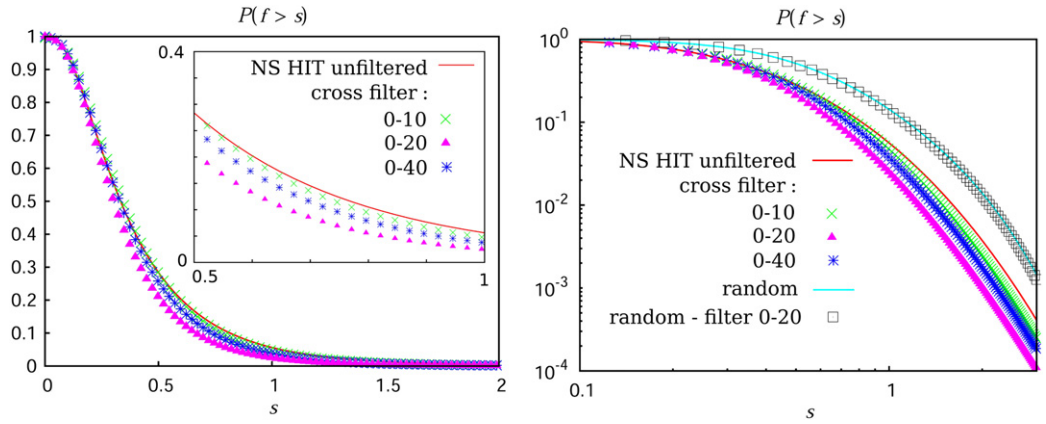

Fig. 6. Survival probability of the normalized vortex stretching function in a high pass filtered isotropic turbulent field. CROSS filter, see in Fig. 4 the blue region. Left panel: Linear–linear plot. Right panel: Linear–log plot. Comparison between the randomized, high pass filtered and unfiltered field and the Navier–Stokes isotropic field (unfiltered and high pass filtered samples).

By varying the value of the threshold, k_{MIN}, it is possible to consider different scale ranges. The ranges 0–10, 0–20, 0–40 are compared in Fig. 6 and in the left panel of Fig. 9. The first filtering affects the energy-containing range, while the other two also include a part of the inertial range, which is visible in Fig. 1.

The plots in Fig. 6 have coherent behavior. The survival function S for the 0–10 filtering is slightly below the values of the distribution of the unfiltered turbulence. This trend is confirmed by the other two filterings, and the reduction grows as the threshold k_{MIN} increases. The high-pass filter has the effect of *decreasing* the statistical values taken by $f(x)$ in the domain. The wider the filtered range, the higher the effect on f.

As far the randomized field is concerned, two things should be noted. First, the survival function of the normalized vortex stretching is twice to four time higher than that of the natural NS field, either unfiltered or filtered. In practice, it seems to be an upper bound for the set of the unfiltered, high pass and band cut filtered NS fields here considered. Second, the survival function of the randomized field is very little affected by the filtering. This is an effect which can be explained by the reduced presence of flow structures induced by the randomization. In Fig. 7, one can observe a zoom of the difference between the survival distributions of the randomized unfiltered and filtered fields. For instance, around $s = 1$, where a variation of 60%–80% can be seen for the NS field, see Figs. 6 and 8, the randomized case shows a few % of variation only.

To summarize, for the Navier–Stokes velocity fluctuation it is possible to say that when we reduce the weight of the large-scale structures (layers, filaments or blobs), the local vortex stretching–tilting intensity decreases with respect to the vorticity magnitude. On average, the values of $f(x)$ go down. The wider the

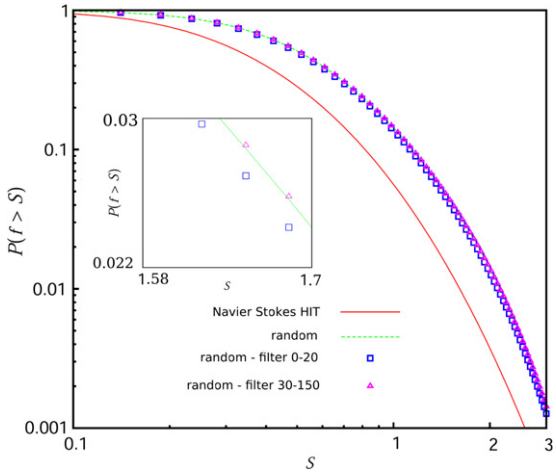

Fig. 7. Survival probability of the normalized vortex stretching–tilting function for the unfiltered isotropic turbulent field (red line), of the corresponding randomized field (dashed green line) obtained by randomizing the phase of the velocity Fourier transform by using a uniform distribution while respecting the periodicity, and of the high pass cross filter of the randomized field (squares) and band cut filter of the randomized field (triangles). Note that the randomized field is very little affected by the filtering.

range affected, the lower the probability value becomes. This suggests that the large scales contribute more to the vortex stretching–tilting (the numerator of f) than to the magnitude of the vorticity fluctuation (the denominator of f). It should be noted that this trend is consistent with the results in [26]. This consistency also includes results relevant to the behavior of the vortex stretching

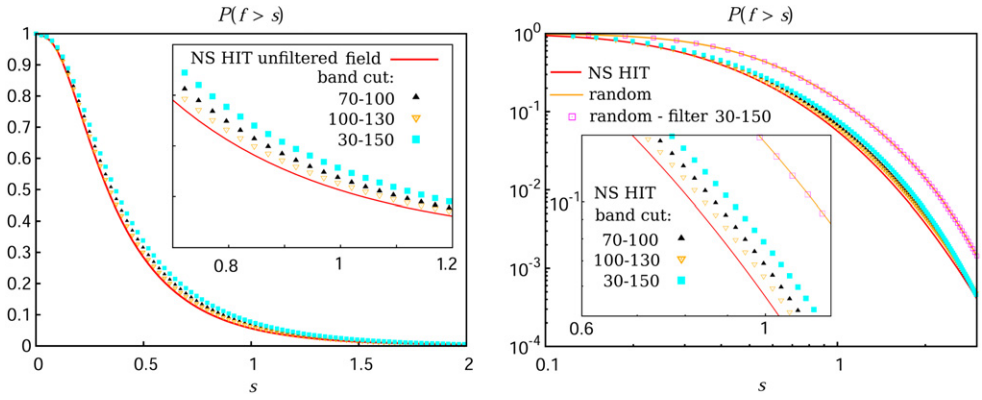

Fig. 8. Survival probability of the normalized vortex stretching function in a band cut filtered isotropic turbulent field. CROSS filter, see in Fig. 4 the red region. Left panel: Linear–linear plot. Right panel: Linear–log plot. Comparison between the randomized, band cut filtered and unfiltered, field and the Navier–Stokes isotropic field (unfiltered and band cut filtered samples).

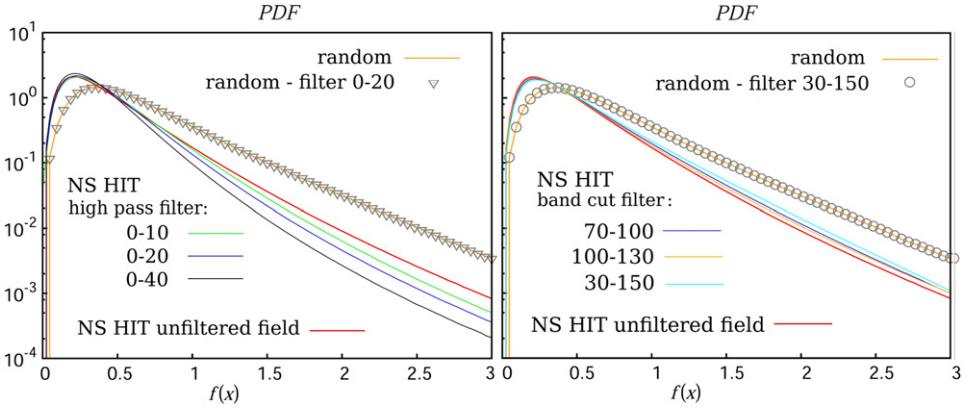

Fig. 9. PDF's of the normalized vortex stretching function. Left panel: high pass CROSS filtered isotropic turbulent field, randomized unfiltered and high pass filtered (0–20) fields. Right panel: band cut filtered isotropic turbulent field, and randomized, unfiltered field and band cut (30–150) filtered fields.

fluctuation and of the vorticity magnitude in boundary layer turbulence, see Figs. 6 and 9 in [15]. For the wider range 0–40, a decrease of 30% in the cumulative probability is observed for a vortex stretching–tilting of about one half of the local vorticity. The decrease goes up to 80% when statistically the vortex stretching–tilting has the same magnitude of the vorticity, that is f is close to 1, see Fig. 6.

Let us now consider the behavior of $f(x)$ when the inertial and dissipative ranges are affected by the filtering, namely a band-stop filtering. In this case, the band width can be extended to obtain a low pass filtering.

This filter can be obtained by reducing the contribution of a variable band (see Fig. 5, part in red)

$k_{MIN} < k_1 < k_{MAX}$ or $k_{MIN} < k_2 < k_{MAX}$ or

$k_{MIN} < k_3 < k_{MAX}$.

This yields the filter function g_{bs}

$$g_{bs}(\underline{k}) = \prod_i \overline{\phi}(k_i; k_{MIN}, k_{MAX}), \tag{5}$$

$$\phi(k_i; k_0) = \frac{1}{1 + e^{-(k_i - k_0)}},$$

$$\overline{\phi}(k_i; k_{MIN}, k_{MAX}) = [1 - \phi(k_i; k_{MIN})] + \phi(k_i; k_{MAX}).$$

The effects of the application of this band-stop filter on the survival probability $P(f(\mathbf{x}) \geq s)$ are shown in Fig. 8 and in the right panel of Fig. 9.

Let us now consider the inertial range in an *extended way*, which includes the $-\frac{5}{3}$ range plus all the scales which are not yet highly dissipative. The different bands are the 30–150 intermediate-inertial/small scale filtering, the 70–100 small scale inertial filtering, the 100–130 near dissipative, the 150–330 dissipative scale filtering. Once again all the filtered ranges induce the same effects: for $s < 1/2$, a slight increase of about 20% in the survival probability. For higher values, $0.5 < s < 2$, the most effective result is obtained filtering over the intermediate-inertial/small scale range, $30 < k < 150$. In this case, an increase of about 60% is observed for $s = 1$ and of about 80% for $s = 1.5$.

This highlights the fact that the structures of the inertial range contribute more to the intensity of the vorticity field than to vortex stretching and tilting. The general trend is inverted with respect to the case of the high pass filtered turbulence and this can be confirmed, with slight differences, as long as we enlarge the amplitude of the filtering band to get closer to the dissipative range. Finally, moving toward the dissipative range ($150 < k < 330$), the band-stop filter becomes a sort of low-pass filter. By filtering these wave numbers, although we have removed the contribution of more or less the highest 200 wave-numbers, see Fig. 1, the effect in the survival distribution is negligible and, since not graphically perceptible, has not been plotted in Fig. 8 and in the right panel of Fig. 9.

To see the effect of the filters on the vortical structures, the vorticity magnitude has been visualized in two ways. The first is a volume rendering of the surfaces where one of the vorticity components is close to the root mean square value, see Fig. 10. The instantaneous field we are considering is homogeneous and isotropic, so all the components are statistically alike and it suffices to observe one component only. In panel (a) the unfiltered field is visualized and a complex picture made of an elongated, thick, sleeve-like structures which are enfolded and twisted can be seen. In panel (b)

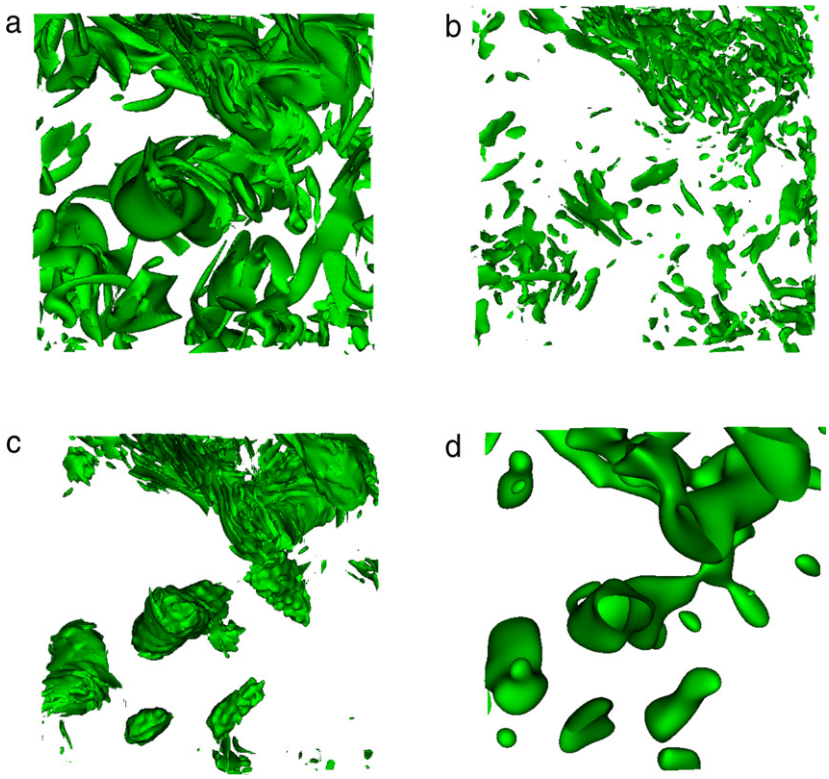

Fig. 10. Three dimensional visualization of the surfaces where one vorticity component has the nondimensional value 17.5. $Re_\lambda = 280$, for an overview of statistical data see Table 1. Panel (a): unfiltered field; panel (b): the wave number range 0–20 is filtered out by using the high-pass cross filter, panel (c): the wave number range 30–150 is filtered out by using the band-stop cross filter; panel (d): the wave number range 30–infinity is filtered out by using the low-pass cross filter, i.e. by letting $k_{MAX} \to \infty$, see Eq. (5). The visualization shows a 256^3 portion of the numerical field simulated on a 1024^3 point grid. The field is visualized by means of VisIt (https://wci.llnl.gov/codes/visit/).

the structures with at least one wavenumber component below 20 are smoothed out, see Eq. (4). One here sees a more sparse distribution of mostly elongated and nearly flat structures with a much shorter length with respect to panel (a). The mutual folding and twisting seems reduced. This image is related to the survival distribution in Fig. 5, where a depression of vortex stretching–tilting over the vorticity magnitude is reported for ratio values above 0.3. Panel (c) shows the band-stop filtered field, where wavenumbers in between 30 and 150 are smoothed out. Basically, most of the inertial and larger dissipative structures are removed. Here, it is interesting to observe that the surface is much more corrugated than in panel (a), which leaves a definitive view of the small scale above wavenumber 150. Some of these structures are elongated, others are globular. The image does not discourage the idea that the large and the very small scales directly interact. Finally, in panel (d) one sees the structures that have at least one wavenumber component in the range 0–30. Here, large unruffled structures which are mainly globular can be seen. The images in panels (c) and (d) represent instances of the statistical situation described in Fig. 8, where the survival ratio of the vortex stretching and vorticity intensities is enhanced with respect to the natural situation. Thus, it seems that the partial absence of the inertial range amplifies the vortex stretching–tilting process. It should also be noted that the density of flow structures is distributed in almost the same way in all the panels, though the shape and typology of the structures is different.

We have tried to visualize the filtering effect also by means of contour plots and pseudocolor imaging of the vorticity magnitude in a flat section of the 1024^3 *field*, see Fig. 11. Here, in the images in the left column show the contours of iso-surfaces of the vorticity magnitude. Starting from the top, one sees the unfiltered field, the high pass filtered field (the wavenumbers above 20 are kept), the 30–150 band-stop, and the low pass filtered field (the range 30–*infinity* is removed). The contour plot technique is very popular, but, apart from clearly showing the reduction of the turbulence scale size when the large scales are missing, it does not give much information. Essentially, structure contours appear to have the peanut shape which typically hosts vortex dipoles.

In the enlarged views in the central and right columns, the pseudocolor plots are richer in information. Where the larger scales are removed, panels (e) and (f), the survival probability of intense vortex stretching is reduced. The range of variation for the vorticity magnitude is very large, the root mean square value is about seven times smaller than the maximum value. When only the large scales are left, panels (m) and (n), the rms value is about one third of the maximum value and the vortex stretching is enhanced. When the inertial scales are removed, the large scale appears to be wrapped by the small scales. The big dipoles are surrounded by thin wavy-like sheets and the small scales are attached to the large ones. In this situation it is not possible to neglect their direct interaction. In regions where a large scale is missing, the small scales are also missing. Vice versa, in the case the small scales had been sparsely distributed in regions where the large scales are not present and would not have surrounded the large structures in regions where the latter are present, a low level of direct interaction between the largest and the smallest scales could have been inferred.

To complement the understanding of the visualization in relation to the anisotropic filtering here used, we have considered the alignment between the eigenvectors of the strain rate tensor and the direction of the vorticity. Function f in fact, see Eq. (1), can also be written as $f(\mathbf{x}) = \frac{|S|}{|\boldsymbol{\omega}|}[s_i^2(e_i * e_\omega)^2]^{1/2}$ where $|S|$ is the magnitude of the strain rate tensor, s_i are the eigenvalues of the strain rate tensor normalized by $|S|$ ($s_i = \lambda_i/|S|$, see Table 2) and $(e_i * e_\omega)$ is the alignment between the eigenvectors of S_{ij}, denoted e_i, and the direction of the vorticity e_ω. Fig. 12 (left panel) shows the probability density function of the alignment in the reference unfiltered field and in two filtered cases described in this work: the high pass filter where the smallest 20 wavenumbers are removed, see Eq. (4),

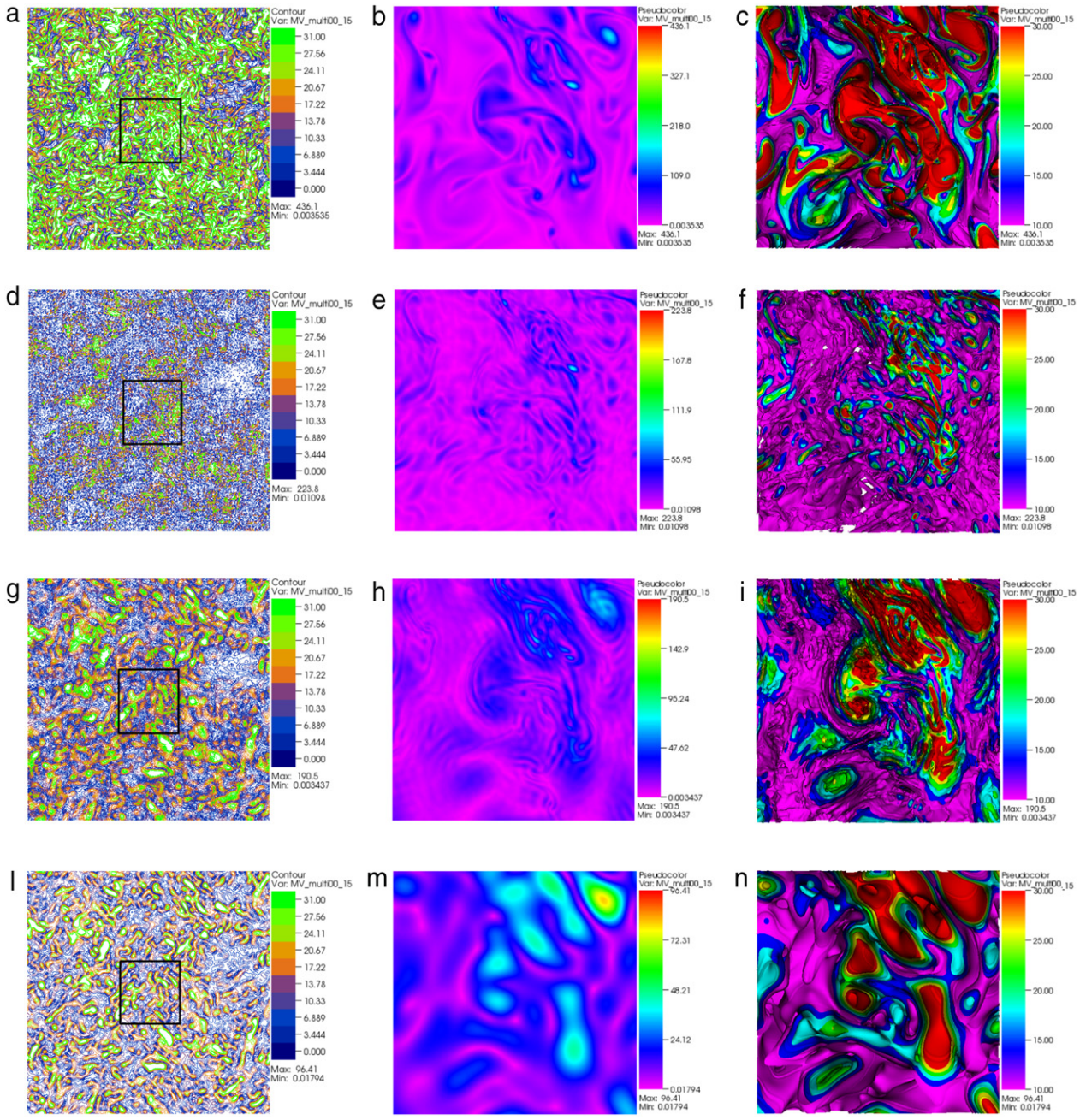

Fig. 11. Visualization of the vorticity magnitude in a section parallel to one face of the computational box. $Re_\lambda = 280$, see Table 1, for an overview of statistical estimates. First row (a, b, c): unfiltered field. Second row (d, e, f): the wave number range 0–20 is filtered out by using the high-pass cross filter. Third row (g, h, i): the wave number range 30–150 is filtered out by using the band-stop cross filter. Fourth row (l, m, n) the wave number range 30–infinity is filtered out by using the low-pass cross filter. In the first column (panels a, d, g, l), it is possible to see the vorticity magnitude contour plots of the entire 1024^3 grid domain. In the second and third column (panels b, e, h, m and c, f, i, n), the pseudocolor plots of a 256^3 portion of the grid (black box in the previous column) are shown. In the third column the range of magnitude values in between 10 and 30 is visualized to show the details of the part of the field where the vorticity magnitude is below its rms value, which is equal to 32. Note that the part above the rms is visualized in the central column, where the entire range of values is included. The Pseudocolor method maps the data values of a scalar variable to color. The plot then draws the colors onto the computational mesh. The field is visualized by means of VisIt (https://wci.llnl.gov/codes/visit/).

and the band-stop filter where wavenumbers 30–150 are removed, see Eq. (5). We first observe that the standard trend of the alignment is not fully spoiled by the filtering. In both filtering cases, eigenvector 2 reduces its alignment, while eigenvector 3 reduces its misalignment. Conversely, eigenvector 1 instead shows a different behavior. In the band-stop filtering case (large scale dominate) eigenvector 1 slightly increases the alignment. In the high-pass filtering, eigenvector 1 reduces the alignment that becomes statistically equal to that of the eigenvector 3. This is confirmed, see Table 2, by considering the ratio among the field averaged strain rate tensor eigenvalues and related component of the enstrophy production, $\langle\sigma_i\rangle/\langle\sigma_{tot}\rangle$, where $\langle\cdot\rangle$ is the average over all the computational domain (1024^3 grid point box), $\sigma_i = \omega^2\lambda_i\cos^2(e_\omega, e_i)$ and $\sigma_{tot} = \langle\sum_i \omega^2\lambda_i\cos^2(e_\omega, e_i)\rangle$. All filters increase the gap between the eigenvalue $\langle\lambda_1\rangle$ and $\langle\lambda_2\rangle$ and the gap between $\langle\lambda_2\rangle$ and $\langle\lambda_3\rangle$. However, when the large scales are missing, eigenvalues 1 and 3 are very close in modulus. The same happens to the modulus of their related enstrophy production components. When the inertial scales and part, or the entire, dissipative range are removed the mutual relation among the eigenvalues and the modulus of the production components changes less with respect to the natural turbulence.

Table 2
Normalized strain rate tensor eigenvalues and normalized enstrophy production computed in the unfiltered and the filtered field.

Principal index axes	Reference unfiltered field ($Re_\lambda = 280$)	Large scales filtered (cross 0–20)*	Intermediate and small scales filtered (cross 30–150)**	Inertial and dissipative scales filtered cross(30–infinity)***	Unfiltered field ($Re_\lambda = 10^4$) [14]
Normalized strain rate tensor eigenvalues $\langle\lambda_i\rangle$					
I	0.54	0.61	0.57	0.56	0.47
II	0.12	0.0013	0.091	0.090	0.06
III	−0.66	−0.61	−0.64	−0.64	−0.53
Normalized enstrophy production $\langle\sigma_i\rangle/\langle\sigma_{tot}\rangle$					
I	1.14	6.31	2.67	2.86	1.06
II	0.66	0.59	0.49	0.45	0.51
III	−0.80	−5.91	−2.16	−2.31	−0.57

* The smallest 20 wavenumbers are filtered out.
** Wavenumbers in the inertial 30–150 range are filtered out.
*** All wavenumbers above 30 are filtered out that behave in much the same way.

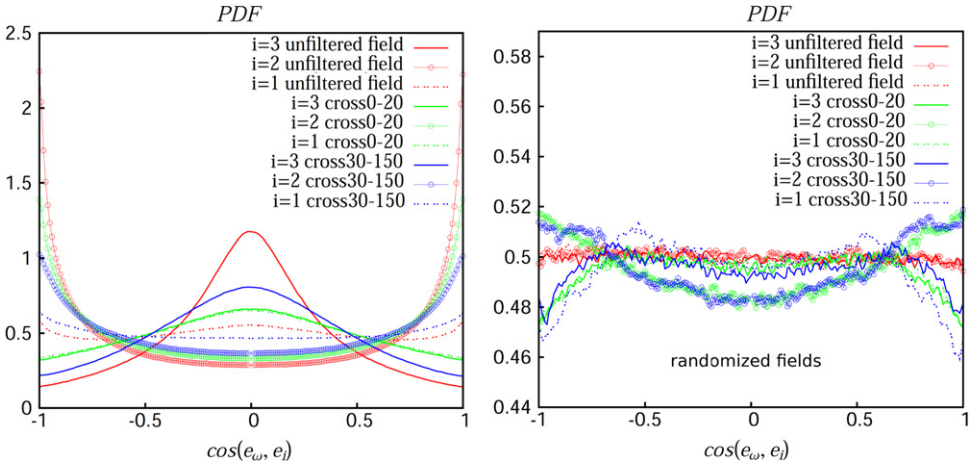

Fig. 12. PDFs of the cosine of the angle between vorticity ($\boldsymbol{\omega}$), and the eigenvector, e_i, of the rate of strain tensor (S_{ij}). Left panel, natural NS field. Right panel, phase-randomized field. The red lines refer to the unfiltered field; the green lines refer to the case where the wave number range 0–20 is filtered out by using the high-pass cross filter; the blue lines refer to the filtering where the wave number range 30–150 is filtered out by using the band-stop cross filter.

In all the three cases the filtering reduces the average values of the largest and intermediate eigenvalue, $\langle\lambda_1\rangle$ and $\langle\lambda_2\rangle$. The situation for the randomized case is represented in the right panel of Fig. 12. While for the unfiltered case the pdf is perfectly flat, the filtering modifies the distribution a little only. The variations in fact are just 1%–2% than those observed in the natural field. Furthermore, there is not a significant difference between the high pass and the band-stop filtering. Eigenvector 2 shows a slightly higher probability of alignment which respect to the eigenvectors 1 and 3, that behave in much the same way.

At this point, let us consider the dual nature of the filaments and sheets, as regards their inclusion in the categories of the small and large scales. A filament which is filtered out by the filter g_{hp} because it has a small wave number (the axial wave number component), will have two large wave number components (the ones normal to the filament axis). Due to these wave components, it will also be filtered out by the filter g_{bs}. A similar situation also holds for the sheets. Thus filaments and sheets are always partially removed when a filtering, either anisotropic or isotropic, is applied. The situation changes with compact structures (the blob), which non ambiguously belong either to the large scale range or to the intermediate-small scale range. The different behavior shown in Figs. 6 and 9 is therefore mainly due to the blob contributions, and, since the variation in the cumulative distributions is opposite and almost of the same magnitude, it is possible to deduce that the partial removal of the background filaments and sheets, which is always done regardless of the filter typology (high pass, band pass, low pass,..), is not statistically relevant. In other words, it appears reasonable to conclude that until a better way to select and remove anisotropic structures such as filaments and sheets is found, first order statistical modification associated to their presence/absence will not be clearly seen.

Lastly, it is interesting to observe that the box filtering of small scales modifies the vortex stretching statistics to a great extent. A field filtered in such a way shows a substantial probability of having more than twice the amount of vortex stretching/tilting compared to the enstrophy [33,34]. In the context of the Large Eddy Simulation methodology, where this kind of filtering is commonly used, it is possible to deduce that, when a fluctuating field shows such a feature, the field is unresolved. As a consequence, it was possible to build a criterion that locates the regions of the field where the inclusion of a subgrid term in the governing equations is advisable (see [33–35]).

In particular, the idea to use survival functions came from an attempt to apply the normalized vortex stretching function to predict when and where to use the sub-grid model in supersonic turbulent fields. We observed that the box filtering typical of LES was modifying the survival distribution in a way that suggested the possibility to guess whether in a computational spatial volume small scales are present or not. It can be noted that the probability of having $f(\mathbf{x}) \geq s$ in the resolved turbulent fields there considered (HIT, jets, channel flow) is always lower than that of the corresponding box volume filtered fields. The values increase when the resolution is reduced. For all the resolutions analyzed, the difference between the probabilities in the filtered and in the fully resolved turbulence is maximum for s about 0.5, while their ratio goes to ∞ for $s \to \infty$,

see, in particular, Fig. 1(a, b) in [34]. This suggested the introduction of a computational threshold so that, when f assumes larger values, the vortex stretching–tilting properties of the unresolved field can be considered artificially large and thus the simulation should benefit from the local activation of a subgrid scale term in the motion equation. In [35], it is shown that this selective LES modifies the dynamic properties of the flow to a lesser extent with respect to the classical LES. In particular, the prediction of the enstrophy, mean velocity and density distributions and that of the energy and density spectra are substantially improved.

4. Conclusions

We have collected a set of statistical information about the vortex stretching intensity normalized by the enstrophy in an isotropic turbulence at $Re_\lambda = 280$ and in a nearly Gaussian field obtained by randomizing with a uniform distribution the phases of the velocity Fourier transform. The randomized field is assumed as a statistical reference and is considered a sufficiently good representation of the Kolmogorov K41 turbulence.

A first result is that the probability of having a vortex stretching/tilting of intensity larger than few times the square of the vorticity magnitude is very low. Then, if compact structures (blobs) in the inertial range are filtered out, it can be seen that the probability of having values of $f(\mathbf{x}) = \frac{|\boldsymbol{\omega}\cdot\nabla\mathbf{U}|}{|\boldsymbol{\omega}|^2}(\mathbf{x})$ higher than a given threshold s increases by 20% at $s = 0.5$, and by 60%–70% at $s = 1.0$. If, on the other hand, larger blobs are filtered, an opposite situation occurs. The unfiltered field is thus a separatrix for the cumulative probability function. This behavior – high fluctuation of the vorticity magnitude → low vortex stretching, and vice versa – agrees with findings observed in a number of laboratory and numerical analyses, [17,26], and also in near wall turbulent flow configurations [10]. It is also observed that, compared with the velocity field, a high intermittency is associated to the normalized vortex stretching f, whose kurtosis is as high as 8 in the natural turbulence (7 in the randomized case).

For the considered estimators, the randomized velocity field show a different behavior. The deconstruction of the field introduced by the randomization is revealed in the fact that, by filtering out different sets of wave numbers, the distributions in the field of the normalized vortex stretching change very little compared to the natural field. In particular, the survival distribution of the normalized vortex stretching is higher than both the unfiltered and filtered NS fields and seems to be an upper bound since it is not sensibly affected by the kind of filtering here tested.

The present observations need to be associated to the non discriminating effect of filtering on filaments and sheets, which is due to their specific nature that cannot be reconciled inside either a category of small or large scales.

The probability density function of the alignments between the strain rate eigenvectors and the vorticity is in part modified by the anisotropic filtering here investigated. In particular, we observe that, though the standard trend of alignments is not fully spoiled, eigenvector 2 reduces its alignment, while eigenvector 3 reduces its misalignment. Conversely eigenvector 1 shows a different behavior. In the band stop filtering case (large scale dominate) eigenvector 1 slightly increases the alignment. In the high pass filtering case (inertial scales dominate), eigenvector 1 reduces the alignment that becomes statistically equal to that of the eigenvector 3. This is confirmed by considering the mutual ratio among the averaged strain rate eigenvalues and the related components of the enstrophy production. Both filters increase the gap between the most extensional eigenvalue $\langle\lambda_1\rangle$ and the intermediate one $\langle\lambda_2\rangle$ and the gap between this last $\langle\lambda_2\rangle$ and the contractile eigenvalue $\langle\lambda_3\rangle$. However, when the large scales are missing, the modulus of eigenvalues 1 and 3 becomes nearly equal, similar to the modulus of the related components of the enstrophy production. Vice versa, the randomized field has no preferential alignment of the rate of strain eigenvectors with the vorticity and the filtering does not modify sensibly this situation.

Acknowledgments

We are grateful to Professor James J. Riley for fruitful discussions. We thank the referees for their constructive reviews and the many suggestions. This work was carried out in cooperation with ICTR, the International Collaboration for Turbulence Research.

References

[1] G.I. Taylor, Production and dissipation of vorticity in a turbulent fluid, Proc. R. Soc. Lond. Ser. A 164 (916) (1938) 15–23.
[2] R. Betchov, An inequality concernig the production of vorticity in isotropic turbulence, J. Fluid Mech. (1) (1956) 497–504.
[3] A.S. Monin, A.M. Yaglom, Statistical Fluid Mechanics, vols. 1–2, The MIT Press, Cambridge, Massachusetts, and London, England, 1971,1975.
[4] H. Tennekes, J.L. Lumley, A First Course in Turbulence, The MIT Press, Cambridge, Massachusetts, and London, England, 1972.
[5] S.B. Pope, Turbulent Flows, Cambridge University Press, 2000.
[6] U. Frisch, Turbulence - The legacy of A.N. Kolmogorov, Cambridge University Press, 1995.
[7] A. Tsinober, An Informal Introduction to Turbulence, first ed., Springer, 2001.
[8] B.W. Zeff, D. Lanterman, R. McAllister, R. Roy, J. Kostelich, D.P. Lathrop, Turbulent mixing of a passive scalar, Nature 421 (2003) 146–149.
[9] G.K. Batchelor, A.A. Townsend, The nature of turbulent motion at large wavenumbers, Proc. R. Soc. Lond. Ser. A 199 (1949) 238.
[10] A. Tsinober, E. Kit, T. Dracos, Experimental investigation of the field of velocity gradients in turbulent flows, J. Fluid Mech. 242 (1992) 169–192.
[11] C.W. Van Atta, R.A. Antonia, Statistics of stretching fields in experimental fluid flows exhibiting chaotic advection, Phys. Fluids 242 (2) (1980) 23.
[12] K.R. Sreenivasan, R.A. Antonia, The phenomenology of small-scale turbulence, Annu. Rev. Fluid Mech. 29 (1997) 435.
[13] T. Ishihara, T. Gotoh, Y. Kaneda, Study of high-Reynolds number isotropic turbulence by direct numerical simulation, Annu. Rev. Fluid Mech. 41 (2009).
[14] T. Ishihara, Y. Kaneda, M. Yokokawa, K. Itakura, A. Uno, Small-scale statistics in high-resolution direct numerical simulation of turbulence: Reynolds number dependence of one-point velocity gradient statistics, J. Fluid Mech. 592 (2007) 335.
[15] Y. Andreapoulos, A. Honkan, An experimental study of the dissipative and vortical motion in turbulent boundary layers, J. Fluid Mech. 439 (2001) 131.
[16] K.K. Nomura, G.K. Post, The structure and dynamics of vorticity and rate of strain in incompressible homogeneous turbulence, J. Fluid Mech. 377 (1998) 65–97.
[17] P.E. Arratia, J.P. Gollub, Statistics of stretching fields in experimental fluid flows exhibiting chaotic advection, J. Stat. Phys. 121 (516) (2005) 805.
[18] A. Tsinober, in: J.C.R. Hunt, J.C. Vassilicos (Eds.), Turbulence structure and Vortex Dynamics, Cambridge University Press, 2000, p. 164.
[19] P. Constantin, I. Procaccia, D. Segel, Creation and dynamics of vortex tubes in three-dimensional turbulence, Phys. Rev. E 51 (1994) 3207.
[20] B. Galanti, I. Procaccia, D. Segel, Dynamics of vortex lines in turbulent flows, Phys. Rev. E 54 (1996) 5122.
[21] M. Kholmyansky, A. Tsinober, S. Yorish, Phys. Fluids 13 (2000) 311.
[22] G. Gulitski, M. Kholmyansky, W. Kinzelbach, B. Lüthi, A. Tsinober, S. Yorish, Velocity and temperature derivatives in high Reynolds number turbulent flows in the atmospheric surface layer. Part 1. Facilities, methods and some general results, J. Fluid Mech. 589 (2007) 57–81.
[23] G. Gulitski, M. Kholmyansky, W. Kinzelbach, B. Lüthi, A. Tsinober, S. Yorish, Velocity and temperature derivatives in high Reynolds number turbulent flows in the atmospheric surface layer. Part 2. Accelerations and related matters, J. Fluid Mech. 589 (2007) 83–102.
[24] G. Gulitski, M. Kholmyansky, W. Kinzelbach, B. Lüthi, A. Tsinober, S. Yorish, Velocity and temperature derivatives in high Reynolds number turbulent flows in the atmospheric surface layer. Part 3. Temperature and joint statistics of temperature and velocity derivatives, J. Fluid Mech. 589 (2007) 103–123.
[25] L. Chevillard, C. Meneveau, L. Biferale, F. Toschi, Modeling the pressure Hessian and viscous Laplacian in turbulence: comparisons with DNS and implications on velocity gradient dynamics, Phys. Fluids 20 (2008) 101504.
[26] P.E. Hamlington, J. Schumacher, W.J.A. Dahm, Direct assessment of vorticity alignment with local and non local strain rates in turbulent flows, Phys. Fluids 20 (2008) 111703.
[27] L. Biferale, G. Boffetta, A. Celani, A. Lanotte, F. Toschi, Particle trapping in three-dimensional fully developed turbulence, Phys. Fluids 17 (2) (2005) 021701/1-4.
[28] A.N. Kolmogorov, Dissipation of energy in the locally isotropic turbulence, C. R. Acad. Sci. URSS 32 (1941) 16–18.

[29] A.N. Kolmogorov, The local structure of turbulence in incompressible viscous fluid for very large Reynolds numbers, C. R. Acad. Sci. URSS 30 (1941) 301–305.
[30] T. Sanada, Energy spectrum and intermittency in two-dimensional decaying turbulence? Progr. Theoret. Phys. 84 (1) (1990) 7–11. http://dx.doi.org/10.1143/ptp/84.1.7.
[31] V. Nikora, D. Goring, R. Camussi, Intermittency and interrelationships between turbulence scaling exponents: phase-randomization tests, Phys. Fluids 13 (5) (2001) 1404–1414.
[32] D. Tordella, M. Iovieno, Numerical experiments on the intermediate asymptotics of shear-free turbulent transport and diffusion, J. Fluid Mech. 549 (2006) 429–441.
[33] D. Tordella, M. Iovieno, S. Massaglia, Small scale localization in turbulent flows. A priori test applied to a possible large Eddy simulation of compressible turbulent flows, Comput. Phys. Comm. 176 (2007) 539. http://dx.doi.org/10.1016/j.cpc.2006.12.004100.
[34] D. Tordella, M. Iovieno, S. Massaglia, Erratum to: small scale localization in turbulent flows. A priori tests applied to a possible large Eddy simulation of compressible turbulent flows, Comput. Phys. Comm. 178 (2008) 883. http://dx.doi.org/10.1016/j.cpc.2008.02.005.
[35] D. Tordella, M. Iovieno, S. Massaglia, A. Mignone, Large-eddy simulation of hypersonic flows. Selective procedure to activate the sub-grid model wherever small scale turbulence is present, Comput. Phys. Comm. 184 (12) (2013) 2651–2661. http://dx.doi.org/10.1016/j.cpc.2013.06.012.